RSC Advances

ROYAL SOCIETY OF CHEMISTRY

www.rsc.org/advances

Table of contents

Photocatalytic activity of hierarchically structured, thermally stable, anatase particles

Andrijana Sever Škapin, Luka Škrlep, Danilo Suvorov and Srečo D. Škapin*

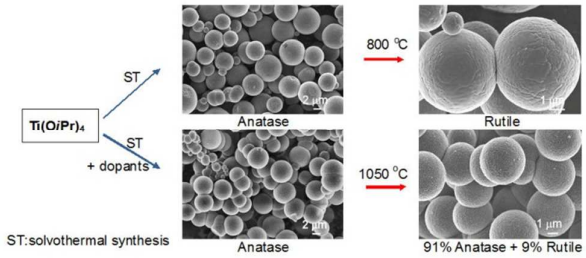

Cite this: DOI: 10.1039/c0xx00000x

www.rsc.org/xxxxxx

ARTICLE TYPE

Photocatalytic activity of hierarchically structured, thermally stable, anatase particles

Andrijana Sever Škapin[a], Luka Škrlep[a], Danilo Suvorov[b], Vojka Žunič[b] and Srečo D. Škapin*[b]

Received (in XXX, XXX) Xth XXXXXXXXX 20XX, Accepted Xth XXXXXXXXX 20XX

DOI: 10.1039/b000000x

In order to avoid the potential health problems associated with nanosized particles, solvothermal synthesis was employed for the preparation of doped and undoped, hierarchically structured, spherical anatase, ranging in size from 2 to 6.4 μm The resulting particles showed a mezoporous microstructure and, consequently, a high specific surface area of up to 208 m^2/g. A detailed SEM analysis confirmed the hierarchical structure of the spheres, consisting of subunits with a size from 10 to 21 nm, depending on the starting composition. For the thermal stabilization of the anatase phase and to slow down the growth of the nanosize particles during heating, various dopants were added to the anatase. As a result, anatase codoped with Ce, Si and Zr exhibited a high thermal stability up to 1050 °C, compared to 700 °C for the undoped anatase. The photocatalytic activities of the synthesized solids were quantitatively evaluated by monitoring the rate of degradation for isopropanol in a gas phase reactor system. Among the samples that were heat treated at 500 °C, the highest photocatalytic activity was exhibited by the Ce-doped sample. In the case of the samples which were heat treated at 1050 °C, the undoped and Ce-doped samples were inactive under UV light, while the samples doped with Ce, Zr and Si exhibited considerable photocatalytic activity.

1. Introduction

Titanium dioxide exhibits many useful optical, electrical and photocatalytic properties, depending on the particle size, the phase composition, the microstructure and the chemical composition. Control of these properties is vital for the desired performance of these materials in applications like sensors, photocatalysis, electronics and pigments.[1] There are reports of photocatalytic activity for all three titania polymorphs, i.e. anatase, rutile and brookite, and their various mixtures.[2-4] However, anatase and mixtures of anatase and rutile are the most commonly used in photocatalytic applications.[1,2] The photocatalytic activity also depends on the specific surface area and the degree of crystallinity. Heterogeneous photocatalytic reactions depend on the energy source, the reactant adsorption, the catalyst activity, the reaction mechanism and the product desorption. All these parameters may influence the ideal properties of the catalytic material for a particular reaction.[1] The chemical composition of the nanosized anatase can have an influence on the particle formation during the synthesis as well as on its morphology, surface acidity and band gap.

Upon heating, the anatase and brookite polymorphs of titanium dioxide eventually transform into the thermodynamically stable rutile form. This usually means a loss of photocatalytic activity, compared to that of the anatase.[4] The transition temperature is important for certain applications where high temperatures are used, like tile or roof-tile production. A mechanism for this phase transition has already been proposed by several authors.[5] For the anatase-to-rutile transformation Reidy et al.[6] suggested a so-called "critical size mechanism". Anatase particles are supposed to grow with increasing temperature; then after reaching a critical size they transform into the rutile phase. In general, the phase-transition temperature of many systems can be controlled by doping. Reidy et al.[7] used silicon and zirconium doping to inhibit the material transport and particle growth during heat treatments. There are also reports of doping with aluminum,[7] cerium,[8-10] silicon,[11,12] sulfur,[13] and phosphorus,[14] to increase the thermal stability of the anatase. It has been shown that the mesoporous anatase particles as well as nanotube arrays are stable to much higher temperatures than non-mesoporous particles.[15-18] Moreover, Grover et al.[19] reported that rice-like anatase could be stable up to 800 °C, however, the particles completely altered their morphology during such thermal treatment. Additionally, in anatase-silica composites the anatase phase is stable at higher temperatures.[20-22]

Anatase nanoparticles can be synthesized by different methods.[1] The solvothermal, non-aqueous method yields materials with several very interesting features, for example, good crystallinity of the products at moderate reaction temperatures. This method is less sensitive to reaction conditions than the syntheses based on aqueous systems.[23] Garnweitner et al.[24] synthesized anatase nanoparticles from titanium isopropoxide in different aldehydes and ketones used as solvents.

Reactions involving a slow aldol condensation with an elimination of the water result in anatase particles with excellent crystallinity. In our investigation we applied the aforementioned method to synthesize the anatase-based nanoparticles, using acetone as the solvent reactant.

The main goals of our investigation were to prepare materials that would (i) exhibit photocatalytic activity even after a heat treatment at very high temperatures, at least 1050 ^{o}C, and (ii) possess non-harmful characteristics. However, it is well known that after a high-temperature treatment, due to the transformation of the anatase into rutile, sintering and particle growth, most of the existing nano-titania tends to lose its photocatalytic activity. The doping shifts the transformation to higher temperatures, whereas the sintering is significantly suppressed. On the other hand, the nanosized TiO_2 particles (< 100 nm) are known to have harmful effects on the cell membrane, and even for non-toxic titania, scientists warn that extreme caution must be used when working with such particles.[25-29]

A compromise was achieved by preparing micron-sized agglomerates showing a hierarchically nanostructured morphology, which nevertheless retain their nanoparticulate nature (high surface area, porosity, etc.) and thus their inherent photocatalytic activity. The influence of the type and the amount of dopant used on the physicochemical properties of anatase is also reported.

2. Experimental section

Preparation of TiO_2-based photocatalysts

Reagent-grade metal alkoxides titanium isopropoxide ($Ti(OiPr)_4$), zirconium-n-butoxide ($Zr(OBu)_4$), tetraethoxysilane ($Si(OEt)_4$) and cerium(III) nitrate hexahydrate ($Ce(NO_3)_3{\cdot}6H_2O$), obtained from Aldrich, were used as received without further purification. In a typical experiment the raw materials, $Ti(OiPr)_4$, $Zr(OBu)_4$, $Si(OEt)_4$ and $Ce(NO_3)_3$, were dissolved in 1 mol of acetone in different mole ratios (Table 1). The prepared starting solution was put into a 100-ml autoclave with a Teflon liner. The autoclave was heated in an oven at 140 °C for 24 h and then left to cool. The obtained yellow-to-amber suspension was filtered and washed with acetone. The filtered product was dried at 110 ^{o}C for 5 h. To remove all the residual organic species and volatiles the solids were heated at a rate of 5 °C/min to 500 °C and left at this temperature for 2 h. For a determination of the temperature of the anatase-to-rutile transformation the samples were additionally heated from 550 ^{o}C to 1050 ^{o}C in 50 ^{o}C intervals and then soaked at each temperature for 0.5 h. The heating rate for these firing experiments was set to 5 °C/min.

Materials characterization

The morphology and the size of the particles were examined with a field-emission scanning electron microscope (FE SEM, Supra 35 VP, Carl Zeiss) equipped with an energy-dispersive spectrometer (EDS, Inca 400, Oxford Instruments). The particle size of the spherical aggregates was obtained from FE-SEM micrographs by applying the software Image Tool for Windows. Phase identification was based on X-ray powder diffraction using a D4 Endeavor, Bruker AXS diffractometer with Cu Kα radiation (λ = 0.154 nm) and a Sol-X energy-dispersive detector within the angular range 2 Θ from 20 to 70 degrees, a step size of 0.02 degrees and a collection time of 5 seconds. The mean crystallite size of the anatase primary particles was determined from the (101) X-ray diffraction peak using the Scherrer equation $d=K\lambda/\beta\cos\Theta$, where a value K=0.9 was used for the shape factor. The surface area of the powders was measured using a BET surface area analyzer (Micromeritics ASAP 2020). The internal microstructures of the prepared spherical, micron-sized, anatase particles were analyzed using a JEOL JEM 2010F transmission electron microscope (TEM) operating at 200 kV. The XPS analyses were performed with a TFA XPS spectrometer (Physical Electronics Inc.) The sample surfaces were excited by X-ray radiation from a monochromatic Al source with an energy of 1486.6 eV. The high-energy-resolution spectra were acquired with an energy analyzer operating at a resolution of about 1.0 eV. For the characterization of the optical properties a UV-Vis-NIR spectrophotometer (Shimadzu UV-3600) equipped with an integrating sphere (ISR-3100, 60 mm) was used. The diffuse reflectance spectra were recorded in the range 200–800 nm under ambient conditions. The band-gap energy for the samples was calculated based on experimentally obtained diffuse reflectance spectra using computer software supplied by Shimadzu.

Photocatalytic study

The photocatalytic activity of the samples was measured by monitoring the degradation of a model organic compound, isopropanol, as well as the acetone formation in a gas medium utilizing FT-IR spectroscopy. Under UV irradiation, the isopropanol, in contact with the photocatalytically active solid substance, oxidizes into acetone and then into several further degradation products. The method enables a quantitative determination of the photocatalytic activity and is described in detail elsewhere.[12,30,31] The light source was a 300-W Xenon lamp (Newport Oriel Instrument, USA) with a light intensity of approximately 25 Wm^{-2} in the λ range 320–400 nm. The spectral power distribution of the light source (Fig. S1) was evaluated by applying a USB2000+ Miniature Fiber Optic Spectrometer (Ocean Optics). It was measured 6 cm from the light source, at the same area as the samples were placed during the UV exposure. The temperature and relative humidity were set to 23±2 ^{o}C and 25±5 %, respectively. For all the measurements the same quantity of sample, 50 mg, was examined and the same initial quantity of liquid isopropanol (3 μl) was injected into the sealed reacting system through a septum. The initial concentration of isopropanol in the sealed reactor was 700 ppm in a gas phase. The photocatalytic activity of the prepared samples was evaluated as the rate constant of the initial acetone formation. The photocatalytic oxidation of isopropanol to form acetone is rapid at room temperature, while the following oxidation of acetone to further degradation products is slower.[32,33] A kinetic model for the calculation of the acetone formation-rate constants has been described in detail elsewhere.[28] The accuracy of the method was estimated to be 1 ppm h^{-1}.

3. Results and discussion

A low-temperature solvothermal synthesis was used in the preparation of anatase-based particles from reaction solutions, with the starting reactant concentrations as summarized in Table 1. Details about the synthesis procedure and the proposed reaction mechanism for anatase formation are described elsewhere.[23,24] Basically, the aldol condensation of acetone takes place, with elimination of water that reacts with titanium isopropoxide forming Ti-O-Ti bonds and isopropanol. Further condensation leads to the formation of oxide nanoparticles. For the purpose of our investigation the doped anatase was prepared by the addition of $Ce(NO_3)_3 \cdot 6H_2O$ and metal alkoxides $Si(OEt)_4$ and $Zr(OBu)_4$ to the starting solution in different ratios. It was expected that a simultaneous hydrolysation of the present alkoxides took place, resulting in Ti-O-M (M = Ti, Si or Zr) bonds under the applied reaction conditions (Fig. S2).

Fig. 1 shows the XRD patterns of the as-prepared TiO_2-based

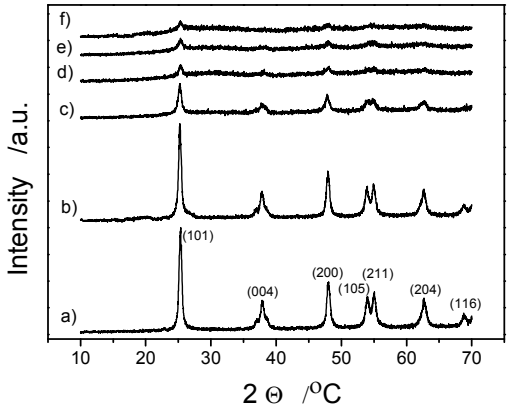

Fig. 1 XRD patterns of the as-prepared TiO_2-based solids: a) sample T (pure TiO_2), b) sample C, c) sample SZ1, d) sample SZ2, e) sample SZ3 and f) sample SZ4.

powders. All the diffraction peaks were matched to the anatase phase (JCPDS card no. 21-1272) and there were no additional peaks corresponding to secondary phases. Single phase nature of the as-prepared TiO_2-based samples was also confirmed by Raman spectroscopy (Figs. S3 and S4). The degree of crystallinity of the non-doped TiO_2 is quite remarkable for such a low synthesis temperature (Fig. 1, pattern a). Similar observations have been reported by other authors.[21] The sample with the cerium addition also shows a similar crystallinity (Fig. 1, pattern b). However, the samples with added Si and Zr in different ratios exhibit diffractograms with broadened XRD peaks, lower intensity and a slightly higher background, suggesting the presence of finer and less-well-crystallized particles (Fig. 1, patterns c-f), due to the incorporation of dopants into the Ti-O network (Fig S5 in the Supporting information).

The as-prepared samples which were additionally calcined for 2 h at 500 oC exhibit similar XRD patterns to those of the samples prior to calcinations. These results suggest that the nanostructure of the agglomerated spherical particles containing the primary nanoparticles and the sample's crystallinity did not change during calcinations.

The information about the particle size and morphology was obtained from a detailed SEM investigation of the prepared solids. Fig. 2 shows a series of FE-SEM micrographs of selected TiO_2-based solids, each sample is presented at two different magnifications. Evidently, all the samples appeared as hierarchically structured spherical clusters. The size of these nearly perfect spheres is summarized in Table 1. The average size of the spherical aggregates for pure anatase (sample T) is determined to be approximately 5.2 μm, whereas for sample C the size increases up to 6.4 μm. However, the opposite trend in the aggregate size can be observed at higher levels of doping. Thus, the highest doped anatase, sample SZ4, forms aggregates with a size of approximately 2.0 μm in diameter (Table 1, Figs. 2a, 2c, 2e and 2g). Higher magnifications of SEM images clearly reveal that the spherical aggregates are mesoporous and that they consist of smaller subunits. A mesoporous assembly of the spherical aggregates was confirmed by SSA measurements, which showed that the average pore size was 3-5 nm. The pure anatase-type TiO_2 exhibits individual nanocrystallites with a

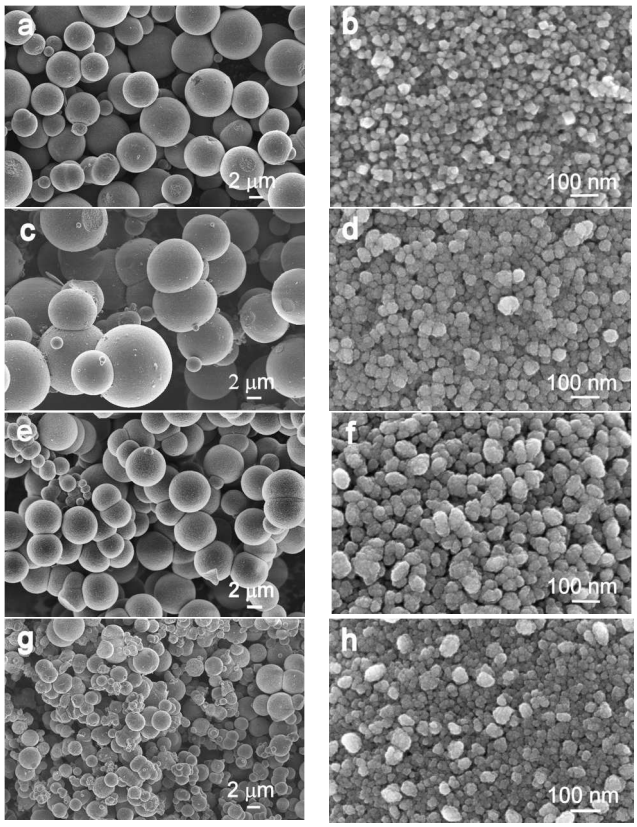

Fig. 2 FE-SEM micrographs of the samples heat treated at 500 °C: a and b) sample T, c and d) sample C, e and f) sample SZ3, and g and h) sample SZ4.

mean size of 21 nm (Fig. 2b); however, the doped samples have larger, nearly spherical subunits, up to approximately 70 nm in diameter, which are composed of even smaller, densely packed, primary nanocrystallites of a size up to 11 nm (Table 1, Figs. 2d, 2f and 2h). Obviously, the crystallite size decreases significantly with dopant content. However, upon adding ZrO_2 to anatase, the opposite effect was reported. Specifically, pure anatase and anatase doped with 10 mol% of ZrO_2 formed 9-nm- and 13-nm-

sized particles, respectively.[34] Finally, according to the literature data, SiO_2 and Ce_2O_3 additions have no significant effect on the size of anatase-type crystallites.[21,35]

The specific surface area of pure TiO_2 is 65 m^2/g and this value decreases with the addition of 0.1 % Ce to 55 m^2/g (sample C); however, larger amounts of dopants result in proportionally more porous agglomerates, and thus, the sample SZ4 shows the highest SSA value of 208 m^2/g (Table 1).

Microspherical-doped TiO_2-based structures were further analyzed using EDS analyses. At least seven measurements on different spheres were carried out for each sample. The analysis of pure TiO_2 and TiO_2 with 0.1 % of Ce addition shows only the presence of Ti and O (Fig. 3, spectra a). The amount of Ce in the sample C is too low to be qualitatively identified by EDS. The results of the analysis of highly doped TiO_2 are slightly scattered, since the shapes of the analyzed spherical objects were far from ideal for such an analysis. Nevertheless, in the co-doped samples Ti cations along with Si and Zr remain in similar proportions as used when preparing the initial mixture (Fig. 3, spectra b and c).

Table 1: Nominal compositions of the starting mixtures of the metal cation concentrations for the preparation of anatase-based samples and their morphological characteristics after calcination for 2 h at 500 °C and the specific surface area for selected samples calcined at 1050 °C

Sample ID	Dissolved moles of the reactants into 1 mol of acetone				Average aggregate size [μm]	Primary particle size [nm]	BET specific surface area [m^2/g]	
	$Ti(OiPr)_4$	$Si(OEt)_4$	$Zr(OBu)_4$	$Ce(NO_3)_3$			500 °C	1050 °C
T	0.1000	0	0	0	5.6± 2.3	21	65	n.a.
C	0.1000	0	0	0.0001	6.4 ± 2.5	16	55	n.a.
SZ1	0.0890	0.0084	0.0026	0.0001	4.7± 2.9	14	152	0.7
SZ2	0.0861	0.0086	0.0053	0.0001	3.4± 1.9	14	158	6.5
SZ3	0.0812	0.0163	0.0025	0.0001	2.8± 1.4	11	194	4.3
SZ4	0.0782	0.0167	0.0051	0.0001	2.0± 1.2	10	208	14.5

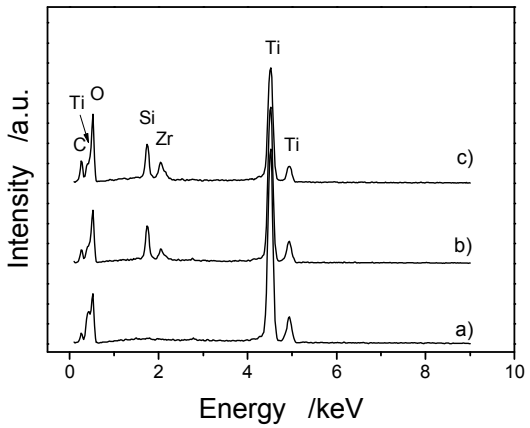

Fig. 3 Characteristic EDS spectra with a qualitative elemental analysis of TiO_2-based microspheres for the selected samples: a) C, b) SZ3 and c) SZ4.

The results shown above suggest that dopants may either enter into the anatase crystal structure or are concentrated on the surface of the primary anatase crystallites. The possibility that dopants may have precipitated as crystallized, discrete phases was also examined by routine X-ray mapping EDS analysis on many locations of the analyzed samples, but the final results did not confirm the formation of discrete phases such as SiO_2 or ZrO_2.

XPS was used to study the chemical state of the dopants Si and Zr on the surface of the samples calcined at 500 °C, whereas the amount of added Ce is too small to be detected. Fig. S5a shows the Si 2p spectra from the sample SZ4, where a single peak corresponding to the bonding energy of Si at 102.1 eV is present. Since the typical bonding energy of Si in SiO_2 is around 104 eV, we can conclude that Si forms Si-O-Ti bonds. The spectra of Zr 3d in Fig. S5b shows a peak with a binding energy at 182.3 eV that can be assigned to the Zr^{4+} valence state in the ZrO_2.

Based on lattice-parameter measurements, many authors have proposed that a certain amount of Si^{4+} may incorporate into the anatase crystal structure.[22,36,37] In contrast, Hirano et al.[21] state that SiO_2 and anatase form a TiO_2/SiO_2 composite, where SiO_2 coexists as an amorphous phase over the anatase crystalline nanoparticles. Similarly, it has been proposed that the CeO_{2-x} that

co-precipitates with anatase does not incorporate into the anatase crystal structure due to the much larger ionic radius of Ce^{3+} and Ce^{4+} (r_{Ce3+}=0.103 nm and r_{Ce4+}=0.093 nm) compared to that of Ti^{4+} (r_{Ti4+}=0.068 nm), thus forming a surrounding amorphous phase.[8,35] In the anatase–ZrO_2 system, up to approximately 40 mol% of TiO_2 can be substituted by Zr and a monoclinic ZrO_2 as a secondary phase is detected at a content of 50 mol% ZrO_2,[34] however Zhang at al.[38] reported that a $ZrTiO_4$ as a secondary phase was detected at 20 mol% ZrO_2. Our measurements of the anatase lattice parameters a and c of the heated samples at 500 °C show a slight variation of the parameters with increasing doping level, where a varies between 0.378 and 0.379 nm and c within 0.953 and 0.951 nm.

TEM analyses were applied in order to observe the internal structure of the micron-sized anatase particles. Since the as-prepared particles were not suitable for a TEM analysis due to their large size (Fig. S6), they were mixed with epoxy resin and applied between two Si wafers and further treated as a bulk sample by thinning, dimpling and ion milling. TEM micrographs of the particles revealed that the micron-sized anatase particles consisted of nanosized, primary crystallites that are partially surrounded by pores and thus exhibited an open mesoporosity (Fig. 4). The results support the conclusions based on the SEM and BET analyses.

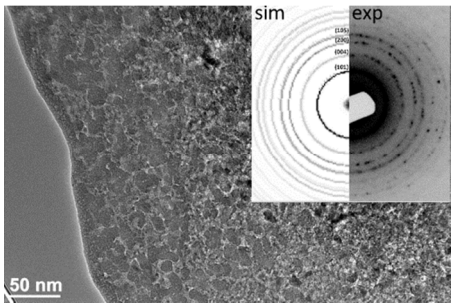

Fig. 4 Bright-field TEM image and corresponding SAED pattern of the sample SZ4 (thin layer on the surface of the particle is the epoxy resin).

The transformation of anatase to rutile (A-R) was reported to be an irreversible first-order process due to the metastability of the anatase structure and is associated with a volume shrinkage of approximately 8 %. The transformation temperature, reported to be higher than 400 °C, depends on several factors, such as the presence of foreign ions, the atmosphere, the method of synthesis, the thermal treatment, the sample form (bulk, film), the grain size, etc.[5,21,39,40] Since the A–R transformation requires relatively high energies for nucleation and further cooperative movement it occurs at relatively high temperatures. A side effect of the process is the simultaneous sintering of the primary TiO_2 particles. The A-R transformation in nanocrystalline solids is proposed as a two-step process, consisting of: i) particle agglomeration by grain-boundary diffusion until the critical particle size is reached for transformation, and ii) a spontaneous A-R transformation.[7] In order to determine the thermal stability of the synthesized anatase, the samples were thermally treated at different temperatures from 550 °C to 1050 °C, with a treatment period of 0.5 h at each temperature. The relative amount of the phases present in the fired samples was calculated using the Spurr equation:[41]

$$x_A\ (wt\%) = 100/(1+1.265(I_R/I_A)), \quad (1)$$

where x_A is the anatase weight content, I_A and I_R are the intensities of the X-ray peak of anatase (101) at 2 Θ equal to 25.5 ° and of the rutile peak (110) at 2 Θ equal to 27.6°. As expected the lowest transformation temperature was exhibited by pure TiO_2. Fig. 5a shows the XRD spectra of the sample T, calcined at 700 °C, 800 °C and 850 °C. The anatase structure is stable up to 700 °C, and at 800 °C the anatase partially transforms to rutile in the amount of 75 % (Table 2), whereas at 850 °C only the rutile is present. Fig. 5b shows XRD patterns for all the presented samples heated at temperatures, where along with the anatase phase, the rutile phase was also found for the first time during the heating procedure (heated from 550 °C to 1050 °C in 50 °C intervals for 0.5 h at each temperature). The sample C (TiO_2 doped with Ce) is stable up to 900 °C; however, at 950 °C it shows a two-phase microstructure with 16 % of rutile (Fig. 5b, Table 2).

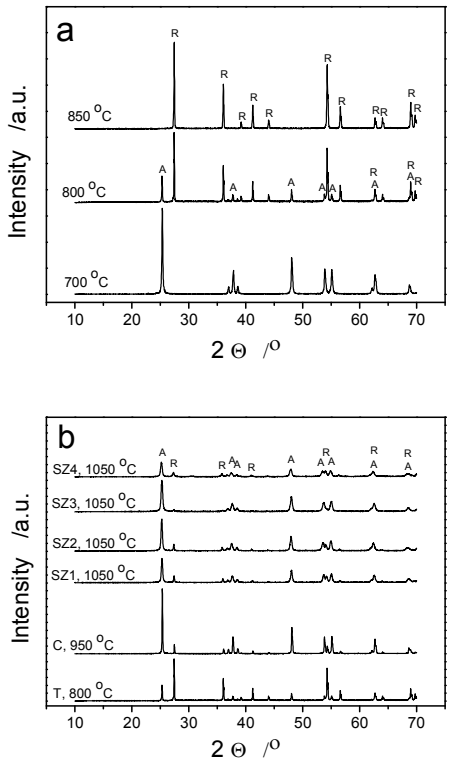

Fig. 5 XRD patterns of heat-treated samples: a) T (pure anatase) at different temperatures (700 °C, 800 °C and 850 °C) and b) T (800 °C), C (950 °C) and SZ1, SZ2, SZ3 and SZ4 (1050 °C).

The samples doped with various dopant amounts show a higher thermal stability, up to 1000 °C. Firing at 1050 °C results in a partial anatase transformation into rutile, whereby the amount transformed depends on the starting composition (Table 2). The lowest amount of rutile phase (9 %) was found in the sample SZ3. It should be stressed that the XRD pattern showed no secondary phases, even when larger amounts of Si- and Zr-based dopants were added to the starting compositions, suggesting that the dopants entered into the anatase crystal structure.

Table 2 The share and mean size of the primary particles of the anatase phase in the heat-treated samples

	Samples					
	T	C	SZ1	SZ2	SZ3	SZ4
T [^{o}C]	800	950	1050	1050	1050	1050
x_A [wt%]	25	84	82	78	91	71
d_A [nm]	71	60	29	28	24	23

The mean size of the primary anatase particles, as determined by Scherrer's equation in the heat-treated samples exhibiting rutile as a secondary phase, decreases from 71 nm for pure TiO_2 (sample T) to 23 nm for the sample SZ4 (Table 2).

Figs. 6 and 7 show micrographs of the fired samples in which a partial and/or complete A-R transformation has occurred. It is clear that after the transformation the TiO_2 retains the spherical shape of the particles. Furthermore, a detailed SEM investigation of the samples revealed that the transformation takes place through the bulk of an individual spherical particle, accompanied by the growth and sintering of the primary anatase particles. Thus, on the surface of the samples T and C, fired at 800 ^{o}C and 950 ^{o}C, respectively, anatase particles/grains with an estimated average size ranging from 25 to 150 nm are observed (Figs. 5b and 7b). It is obvious that the primary particles are partially sintered, forming a non-porous spherical body. However, higher-level doped TiO_2 (samples SZ1–4), heated at 1050 ^{o}C for 0.5 h, still possesses a partially mesoporous structure, although the primary particles are grown from 15 nm to 100 nm and these subunits are partially bridged (Figs. 7d and 7f). The size of the subunits in the heated samples, determined from the XRD patterns using Scherrer's equation (Table 2), fits within these, rather wide, size distributions. This observation is in agreement with the recently proposed two-step mechanism of the A-R transformation, consisting of anatase particle growth and a transformation process of primary anatase nanocrystallites. The

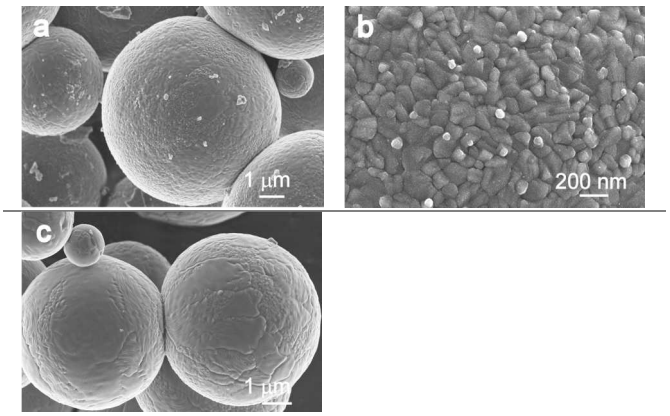

Fig. 6 FE-SEM micrographs of the sample T heat treated for 0.5 h at: a and b) 800 ^{o}C, containing 75 % of rutile and c) 850 ^{o}C, consisting of pure rutile.

samples fired above the transformation temperature in which only the rutile phase was detected, appeared as spherical particles with a mostly smooth surface. These spheres are built up of larger rutile grains with well-developed grain boundaries. The size of the rutile grains depends on the size of spheres and may range from few hundreds of nm to a few μm (Fig. 6c). The BET measurements of the co-doped samples heated at 1050 oC (Table 1) show an increase in the specific surface area by increasing the amount of dopants and thus confirming the SEM results, i.e., that the heavily doped anatase still exhibits a partially open porosity. The band-gap energies of the prepared photocatalysts were determined from the diffuse reflectance spectra (**Error! Reference source not found.**. S7) using the Kubelka-Munk transformation (Table S1). The obtained results show that the band-gap values for the samples are around 3.2 eV and that the dopants have a minor influence on the size of the band gap.

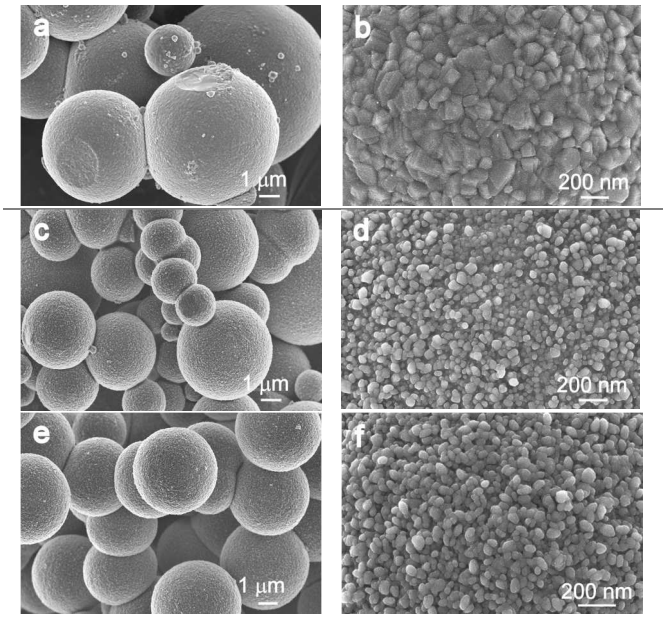

Fig. 7 FE-SEM micrographs of the samples heat treated at high temperatures for 0.5 h: a and b) C at 950 ^{o}C, c and d) SZ2 at 1050^{o}C, and e and f) SZ3 at 1050^{o}C.

The samples were further analyzed with regard to their photocatalytic activity. The latter was measured by monitoring the initial acetone formation during the photocatalytic degradation of isopropanol in the presence of the samples and UV light. The photocatalytic-activity results of the doped and non-doped samples are shown in Table 3 and in Figs. 8a and 8b. The formation of acetone during the photocatalytic degradation of isopropanol in the presence of samples heat treated at 500 ^{o}C is illustrated in Fig. 8a, while the formation of acetone in the presence of samples that were additionally heated from 550 ^{o}C to 1050 ^{o}C in 50 ^{o}C intervals, maintaining each temperature for 0.5 h, is shown in Fig. 8b. In all the photocatalytic measurements at the beginning of the experiment the UV lamp was switched off to achieve an adsorption–desorption equilibrium for the injected isopropanol. The time zero in both Figs. represents the point when the UV lamp was switched on. The photocatalytic activity

of the powders was assessed according to the value of the rate constant representing the oxidation of isopropanol into acetone. This reaction is usually considered a zero-order reaction, while the further oxidation can be assumed to be a first-order reaction.[30,31]

In the present context we are merely interested in the relative change of the rate constant of the isopropanol oxidation into acetone, which is a measure of the photocatalytic activity. The results for different samples are summarized in Table 3. It is clear that the heat treatment of the doped and non-doped samples at 500 °C results in very good activity. The activity of the non-doped TiO_2 was found to be 370 ppm h^{-1}, which is comparable with the value of the photocatalytic activity (337 ppm h^{-1}) of the reference sample Hombikat UV 100 (anatase nanopowder), which was presented in a previous paper.[42] The doping with Ce increases the activity by almost three times, while the activity is increased in a similar way for samples SZ1 and SZ2. For sample SZ3 the activity is approximately the same as for the non-doped TiO_2, while in the case of sample SZ4 the activity is slightly decreased. However, the photocatalytic activity of the samples, when additionally treated at 1050 °C, is rather different. The samples T and C, when treated at 1050 °C, show basically no photocatalytic activity. On the other hand, all the doped samples, SZ1, SZ2, SZ3 and SZ4, retain some activity (from 10 to 54 ppm h^{-1}) even after being heat treated at 1050 °C. This is consistent with the results of the morphological and structural investigations. For example, the highest activity after heat treatment at 1050 °C (54 ppm h^{-1}) is observed in the sample SZ3, the one with the largest amount of untransformed anatase.

Table 3 Photocatalytic activity of the samples heat treated at 500 °C and the samples additionally heat treated at 1050 °C

Sample ID	Rate constant of the initial acetone formation [ppm h^{-1}]	
	Samples heated at 500 °C	Samples additionally heated at 1050 °C
T	370	0
C	907	0
SZ1	679	10
SZ2	477	47
SZ3	364	54
SZ4	174	45

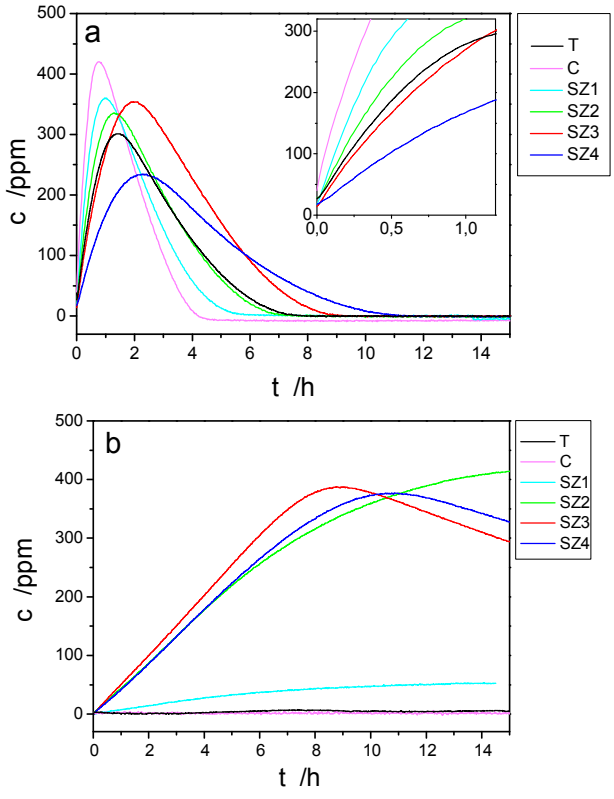

Fig. 8 Acetone formation curves in the presence of samples heat treated at: a) 500 °C for 2 h. The inset shows a magnified part of the curves at the beginning of the photocatalytic process and b) 500 °C for 2 h and additionally heated at 1050 °C for 0.5 h (initial concentration of isopropanol was 700 ppm, T=23±2 °C and relative humidity = 25±5 %).

4. Conclusions

Micrometer-sized, spherical, mesoporous particles of un-doped and doped anatase were successfully prepared by the solvothermal synthesis method in acetone media. Hierarchically assembled, spherical particles from nanosized primary crystallites were formed under certain experimental conditions in the absence of templating agents. Heat-treatment experiments conducted on the prepared solids confirmed that the used dopants increase the temperature of the anatase-to-rutile transformation. Thus, the pure anatase started to transform into rutile above 700 °C; the anatase with the addition of 0.1 mol% Ce, above 900 °C; while the anatase co-doped with Si and Zr is stable up to 1000 °C. The smallest amount of transformed anatase at 1050 °C was found for sample SZ3, containing 16.3 mol% Si, 2.5 mol% Zr and 0.1 mol% Ce.

Acknowledgements

The authors gratefully acknowledge dr. Janez Zavašnik and Ms Andreja Šestan BSc. for their help in performing the TEM analysis, and dr. Janez Kovač for the XPS analysis.

References

1 X. Chen and S. S. Mao, Chem. Rev., 2007, 107, 2891-2959.
2 S. Yin, Y. Aita, M. Komatsu and T. Sato, J. Eur. Ceram. Soc., 2006, 26, 2735-2742.
3 S.Yin, K. Ihara, M. Komatsu, Q. Zhang, F. Saito, T. Kyotani and T. Sato, Solid State Comm., 2006, 137, 132-137.
4 S. Bakardjieva, J. Šubrt, V. Štengl, M. J. Dianez and M. J. Sayagues, Applied Catalysis B: Environmental, 2005, 58, 193–202.
5 R. D. Shannon and J. A. Pask, J. Am. Ceram. Soc., 1965, 48, 391-398.

6 D. J. Reidy, J. D. Holmes and M. A. Morris, J. Eur. Ceram. Soc., 2006, 26, 1527-1534.

7 D. J. Reidy, J. D. Holmes and M. A. Morris, Ceram. Int., 2006, 32, 235-239.

8 Y.-H. Xu, H.-R. Chen, Z.-X. Zeng and B. Lei, *Appl. Surf. Sci.*, 2006, 252, 8565-8570.

9 Q.-Z.Yan, X.-T. Su, Z.-Y. Huang and C.-C. Ge, *J. Eur. Ceram. Soc.*, 2006, 26, 915-921.

10 R. F. De Farias and C. Airoldi, *J. Non-Cryst. Solids*, 2005, 351, 84-88.

11 H. Kominami, M. Kohno, Y. Matsunaga and Y. Kera, *J. Am. Ceram. Soc.*, 2001, 84, 1178-1180.

12 C. He, B. Tian and J. Zhang, *J. Colloid Interface Sci.*, 2010, 344, 382-389.

13 E. M. Rockafellow, L. K. Stewart and W.S. Jenks, *Applied Catalysis B: Environmental*, 2009, 91 554-562.

14 L. Körösi, S. Papp, I. Bertóti and I. Dékány, *Chem. Mater.*, 2007, 19, 4811-4819.

15 D. J. Reidy, J. D. Holmes and M. A. Morris, *J. Mater. Chem.*, 2005, 15, 3494-3500.

16 K. Charette, J. Zhu, S. O. Salley, K. Y. S. Ng and D. Deng, *RSC Adv.*, 2014, 4, 2557-2562.

17 D.-W. Lee, S.-J. Park, S.-K. Ihm and K.-H. Lee, *Chem. Mater.*, 2007, 19, 937-941.

18 B. M. Rao and S. C. Roy, *RSC Adv.*, 2014, 4, 38133-38139.

19 I. S. Grover, S. Singh and B. Pal, *RSC Adv.*, 2014, 4, 24704-24709.

20 D.-W. Lee, S.-K. Ihm and K.-H. Lee, *Chem. Mater.*, 2005, 17, 4461-4467.

21 M. Hirano, K. Ota and H. Iwata, *Chem. Mater.*, 2004, 16, 3725-3732.

22 D. M. Tobaldi, A. Tucci, A. S. Škapin and L. Esposito, *J. Eur. Ceram. Soc.*, 2010, 30, 2481-2490.

23 M. Niederberger, G. Garnweitner, N. Pinna, and G. Neri, *Prog. Solid State Chem.*, 2005, 33, 59-70.

24 G. Garnweitner, M. Antonietti and M. Niederberger,. *Chem. Commun.*, 2005, 3, 397-399.

25 Y. Nakagawa, S. Wakuri, K. Sakamoto and N. Tanaka, *Mutat. Res.*, 1997, 394, 125-132.

26 P. Amézaga-Madrid, R. Silveyra-Morales, L. Córdoba-Fierro, G. V. Nevaráz-Moorillón, M. Miki-Yoshida, E. Orrantia-Borunda and F. J. Solis, *J. Photochem. and Photobiology B: Biology*, 2003, 70, 45-50.

27 J. Wang, G. Zhou, C. Chen, H. Yu, T. Wang, Y. Ma, G. Jia, Y. Gao, B. Li, J. Sun, Y. Li, F. Jiao, Y. Zhao and Z. Chai, *Toxicology Lett.*, 2007, 168, 176-185.

28 V. H. Grassian, P. T. O'Shaughnessy, A. Adamcakova-Dodd, J. M. Pettibone and P. S. Thorne, *Environ Health Perspect.*, 2007, 115, 397-402.

29 F. Pacheco-Torgal and S. Jalali, *Constr. Build. Mater.*, 2011, 25, 582-590.

30 T. Marolt, A. Sever Škapin, J. Bernard, P. Živec and M. Gaberšček, *Surf.&Coat. Techn.*, 2011, 206, 1355-1361.

31 M. Tasbihi, U. Lavrenčič Štangar, A. Sever Škapin, A. Ristić, V. Kaučič and N. Novak Tušar, *J. Photochem. Photobiol. A: Chemistry*, 2010, 216, 167-178.

32 S. A. Larson, J. A. Widegren and J. L. Falconer, *J. Catal.*, 1995, 157, 611-625.

33 Y. Ohko, A. Fujishima and K. Hashimoto, *J. Phys. Chem. B*,1998, 102, 1724-1729.

34 M. Hirano, C. Nakahara, K. Ota, O. Tanaike and M. Inagaki, *J. Solid State Chem.*, 2003, 170, 39-47.

35 Z. Liu, B. Guo, L. Hong and H. Jiang, *J. Phys. Chem. Sol.*, 2005, 66,161-167.

36 M. K. Akhtar, S. E. Pratsinis and S. V. R. Mastrangelo, *J. Am. Ceram. Soc.*, 1992, 71, 3408-3416.

37 K. Okada, N. Yamamoto, Y. Kameshima, A. Yasumori and K. J. D. MacKenzie, *J. Am. Ceram. Soc.*, 2001, 84, 1591-1596.

38 P. Zheng, Y. Yu, E. Wang, J. Wang, J. Yao J and Y. Cao, *ACS Appl. Mater. Interfaces*, 2014, 6, 4622-4629.

39 R. Rodriguez-Talavera, S. Vargas, R. Arroyo-Murillo, R. Montiel-Campos and E. Haro-Poniatowski, *J. Mat. Res.*, 1997, 12, 439-443.

40 K. C. Song and S. E. Pratsinis, *J. Am. Ceram. Soc.*, 2001, 84, 92-98.

41 R. A. Spurr and H. Myers, *Analytical Chem.*, 1957, 29, 760-762.

42 D. M. Tobaldi, L. Gao, A. F. Gualtieri, A. Sever Škapin, A. Tucci and C. Giacobbe, *J. Am. Ceram. Soc.*, 2012, 95, 1709-1716.

Notes and references

[a] *Slovenian National Building and Civil Engineering Institute, Dimičeva 12, 1000 Ljubljana, Slovenia*

[b] *Jožef Stefan Institute, Jamova 39, 1000 Ljubljana, Slovenia, E-mail: Sreco.Skapin@ijs.si; Fax:+3861 4773875; Tel:+386 1 4773708*

† Electronic Supplementary Information (ESI) available: [details of any supplementary information available should be included here]. See DOI: 10.1039/b000000x/